POLITECNICO DI TORINO
Repository ISTITUZIONALE

Contact analysis of laminated structures including transverse shear and stretching

Original
Contact analysis of laminated structures including transverse shear and stretching / Nagaraj, M.H., Kaleel, I., Carrera, E., Petrolo, M.. - In: EUROPEAN JOURNAL OF MECHANICS. A, SOLIDS. - ISSN 0997-7538. - STAMPA. - 80:(2020). [10.1016/j.euromechsol.2019.103899]

Availability:
This version is available at: 11583/2785779 since: 2020-01-28T08:10:26Z

Publisher:
Elsevier

Published
DOI:10.1016/j.euromechsol.2019.103899

Terms of use:

This article is made available under terms and conditions as specified in the corresponding bibliographic description in the repository

Publisher copyright
Elsevier postprint/Author's Accepted Manuscript

© 2020. This manuscript version is made available under the CC-BY-NC-ND 4.0 license
http://creativecommons.org/licenses/by-nc-nd/4.0/.The final authenticated version is available online at:
http://dx.doi.org/10.1016/j.euromechsol.2019.103899

(Article begins on next page)

09 October 2026

Contact analysis of laminated structures including transverse shear and stretching

M.H. Nagaraj, I. Kaleel, E. Carrera, M. Petrolo
MUL^2 Group, Department of Mechanical and Aerospace Engineering,
Politecnico di Torino, Corso Duca degli Abruzzi 24, 10129 Torino, Italy

Submitted to

European Journal of Mechanics - A/Solids

Author for correspondence:
E. Carrera, Professor of Aerospace Structures and Aeroelasticity,
MUL^2 Group, Department of Mechanical and Aerospace Engineering,
Politecnico di Torino,
Corso Duca degli Abruzzi 24,
10129 Torino, Italy,
tel: +39 011 090 6836,
fax: +39 011 090 6899,
e-mail: erasmo.carrera@polito.it

Abstract

This work presents contact problems of laminated structures via the Carrera Unified Formulation (CUF). The modeling approach makes use of higher-order 1D elements accounting for transverse shear and stretching. The current work considers normal, frictionless contact based on a node-to-node formulation, and the penalty approach to enforce the contact constraints. Numerical assessments compare classical beam theories, higher-order CUF, and 3D finite element models regarding solution accuracy, computational size, and time required for the analysis. The results show the validity of Layer-Wise CUF models to capture both global and local deformations accurately, which is a shortcoming of classical beam theories, and require at least an order of magnitude fewer degrees of freedom and computational time than a full 3D finite element analysis. Particularly relevant are the accurate distributions of transverse shear stress and stretching along the thickness in the perspective of failure analyses.

Keywords: Node-to-Node contact, CUF, multilayer, sandwich

1 Introduction

Contact mechanics is an important aspect of structural analysis as there usually exists a state of static or dynamic contact between various components of a mechanical system. Some instances of contact include meshing gears, forming processes, and the simulation of indentation. An important engineering application of contact is the impact analysis of structures. This is especially relevant due to the increasing use of composite laminated materials in which impacts can cause localized damage and delamination, the latter leading to a severe reduction of the structural mechanical properties.

The numerical modeling of contact is a current issue in the field of computational mechanics [1]. Various techniques have arisen during the last few decades with varying complexity. Early works introduced node-to-node contact algorithms in which the contact constraint acts at the nodal level [2, 3]. Node-to-node algorithms constitute the simplest approach and may have limited applications due to the requirements of a conforming mesh and nodal compatibility between the contacting bodies. The necessity to overcome such restrictions led to the development of contact algorithms based on node-surface interactions in which a constraint on the *slave* node avoid penetration through the *master* surface [4, 5]. Such a class of contact strategies, often referred to as single-pass methods, ensures that the *slave* nodes do not penetrate the *master* surface but has not constraints concerning the nodes of the *master* surface penetrating the *slave* surface. Such methods may not be effective for specific geometries and often fail the contact patch test [6]. This led to the development of two-pass algorithms with a two-way application of the standard node-surface algorithm, i.e., the *master* surface and *slave* node definitions swapped in the second run. While such a technique results in an attractive solution that passes the contact patch test, it often suffers from locking, i.e., over-constraining of the system. For this reason, efforts shifted to surface-based approaches in which the contact constraint acts in an integral or *weak* form over the contact surfaces of the interacting bodies [6–8]. A particular class of surface-based contact algorithms is the mortar method in which the discretization of the *slave* surface defines the interpolation of the contact constraints [1, 9–11].

More recently, researchers have proposed methods to transform non-matching meshes of interacting bodies to enable the use of node-to-node contact algorithms. Such a strategy for tackling the problem of contact aims to exploit the simplicity of node-based algorithms and their low computational cost as compared to surface-based algorithms. Some instances include the use of variable node elements [12], the use of polyhedral elements with sud-dividable polygonal faces [13], and the use of virtual contact elements to interface the two contacting surfaces [14]. All these techniques effectively convert a general non-matching mesh into equivalent discretizations having nodal compatibility at the various interfaces and allowing for the use of classical node-to-node contact formulations.

The high-fidelity numerical modeling of composite structures using 3D FE can involve very high computational costs. Particularly demanding outputs are transverse axial, and shear stresses playing a decisive role in failure initiation and propagation. Contact problems, due to their inherent nonlinearity, can further increase

the computational cost of the analysis. Refined beam theories may address the issue of computational effort given that refined models are available and extensive works by Wriggers et al. on the development of contact algorithms specifically for beams [15–18]. Examples of approaches to refining beam models include the Generalised Beam Theory (GBT) which applies cross-section deformation modes to obtain the deformed configuration [19, 20] and the Variational Asymptotic Method to refine the beam theory [21] with rigorous control of the accuracy. The present work utilizes the Carrera Unified Formulation (CUF) [22]. CUF layer-wise (LW) beam models can obtain accurate stress fields in a computationally efficient manner [23]. The CUF framework has recent extensions to nonlinear problems involving geometrical nonlinearities [24], as well as material nonlinearities [25, 26].

The current work involves the assessment of 1D structural models for contact problems involving composite structures and using CUF [22]. Geometrical constraints based on the non-penetration condition enforce contact between the interacting bodies modeled using higher-order beams based on CUF. The numerical results underline the role of higher-order cross-sectional displacement fields to capture 3D-like stress fields. The paper has the following sections: Section 2 describes CUF in detail, while a brief introduction to contact mechanics and its implementation in CUF via a node-to-node formulation is in Section 3. The numerical assessments are in Section 4, and finally, the conclusions in Section 5.

2 Structural theories and finite element formulation

Given a beam segment, aligned along the y-axis, as shown in Fig. 1, CUF defines its displacement field as

$$\mathbf{u}(x, y, z) = F_\tau(x, z)\mathbf{u}_\tau(y), \tau = 1, 2, \dots M \tag{1}$$

where the expansion function F_τ defines the cross-section kinematics, and $\mathbf{u}_\tau(y)$ is the vector of the generalized displacements. The number of terms in the expansion function is M. The choice of the expansion and the number of terms defines a structural theory. This paper makes use of Taylor and Lagrange expansions, as detailed below.

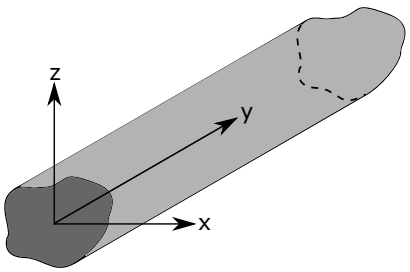

Figure 1: Arbitrary beam element and Cartesian reference frame

Taylor expansion This class of expansion functions, referred to as TE, employs a Taylor series of the type x^i z^i across the cross-section of the beam. The order of the resulting polynomial is N and arbitrary. For instance,

the second-order TE model - N = 2 - is

$$\begin{aligned} u_x &= u_{x_1} + xu_{x_2} + zu_{x_3} + x^2u_{x_4} + xzu_{x_5} + z^2u_{x_6} \\ u_y &= u_{y_1} + xu_{y_2} + zu_{y_3} + x^2u_{y_4} + xzu_{y_5} + z^2u_{y_6} \\ u_z &= u_{z_1} + xu_{z_2} + zu_{z_3} + x^2u_{z_4} + xzu_{z_5} + z^2u_{z_6} \end{aligned} \tag{2}$$

Classical beam models such as the Euler-Bernoulli Beam Theory (EBBT) and Timoshenko Beam Theory (TBT) are special cases of the N = 1 case. In this class of the expansion function, the system unknowns are the displacements and their derivatives till the N^{th} order. More details on the use of the Taylor series as a class of expansion functions in CUF are in [27].

Lagrange expansion In this class of expansion, referred to as LE, Lagrange polynomials define the displacement field over the cross-section. LE results in pure displacement degrees of freedom (DOF) with no rotations or derivatives involved. The displacement field of the 9-node quadratic cross-sectional element (L9) is

$$\begin{aligned} u_x &= \sum_{\tau=1}^{9} F_\tau(x,z) \cdot u_{x_\tau}(y) \\ u_y &= \sum_{\tau=1}^{9} F_\tau(x,z) \cdot u_{y_\tau}(y) \\ u_z &= \sum_{\tau=1}^{9} F_\tau(x,z) \cdot u_{z_\tau}(y) \end{aligned} \tag{3}$$

where u_{x_τ}, u_{y_τ}, u_{z_τ} are translational DOF and F_τ is the Lagrange interpolation function. Further details on the use of LE as a class of expansion function in CUF are in [28].

Finite element formulation The stress and strain vectors are

$$\begin{aligned} \boldsymbol{\sigma} &= \{\sigma_{xx}, \sigma_{yy}, \sigma_{zz}, \sigma_{xy}, \sigma_{xz}, \sigma_{yz}\} \\ \boldsymbol{\varepsilon} &= \{\varepsilon_{xx}, \varepsilon_{yy}, \varepsilon_{zz}, \varepsilon_{xy}, \varepsilon_{xz}, \varepsilon_{yz}\} \end{aligned} \tag{4}$$

The linear strain-displacement relation is

$$\boldsymbol{\varepsilon} = \mathbf{D}\mathbf{u} \tag{5}$$

where $\mathbf{D}$ is

$$\mathbf{D} = \begin{bmatrix} \frac{\partial}{\partial x} & 0 & 0 \\ 0 & \frac{\partial}{\partial y} & 0 \\ 0 & 0 & \frac{\partial}{\partial z} \\ \frac{\partial}{\partial y} & \frac{\partial}{\partial x} & 0 \\ \frac{\partial}{\partial z} & 0 & \frac{\partial}{\partial x} \\ 0 & \frac{\partial}{\partial z} & \frac{\partial}{\partial y} \end{bmatrix}$$

The stress-strain relation is

$$\boldsymbol{\sigma} = \mathbf{C}\boldsymbol{\varepsilon} \tag{6}$$

where $\mathbf{C}$ is the material stiffness matrix. The structure has standard beam elements along the axis using the nodal interpolation functions N_i,

$$\mathbf{u}(x, y, z) = F_\tau(x, z)N_i(y)\mathbf{u}_{\tau i} \tag{7}$$

According to the principle of virtual displacements (PVD),

$$\delta L_{int} = \delta L_{ext} \tag{8}$$

where δL_{int} is the virtual variation of the internal strain energy,

$$\delta L_{int} = \int_V \delta\boldsymbol{\varepsilon}^T \boldsymbol{\sigma} dV \tag{9}$$

$\delta \mathrm{L}_{ext}$ is the virtual work due to external loading,

$$\delta L_{ext} = F_s N_j \delta \mathbf{u}_{sj}^T \mathbf{P} \tag{10}$$

where $\mathbf{P}$ is the external force vector. Via Eqs. (6), (7) and (9), the stiffness matrix reads

$$\delta L_{int} = \delta \mathbf{u}_{sj}^T \mathbf{k}^{ij\tau s} \mathbf{u}_{\tau i} \tag{11}$$

where

$$\mathbf{k}^{ij\tau s} = \int_l \int_A \mathbf{D}^T (N_i(y)F_\tau(x, z))\mathbf{C}\mathbf{D}(N_j(y)F_s(x, z))\ dA\ dl \tag{12}$$

where A and l indicate the axial and cross-sectional domains. $\mathbf{k}_{ij\tau s}$ is a 3×3 matrix and referred to as the Fundamental Nucleus (FN). Its form remains invariant for any given expansion function and order. A detailed explanation of the concept of the fundamental nucleus and its role in CUF is in [22].

3 Contact Mechanics

3.1 Contact kinematics

Let us consider two distinct bodies Ω_i, i = 1,2, as shown in Fig. 2. Two distinct points $\mathbf{X}_1$ and $\mathbf{X}_2$ initially on the boundary of the respective bodies, come into contact due to the applied deformation φ. The position of the points X_i in the current configuration is

$$\mathbf{x}_i = \mathbf{X}_i + \mathbf{u}_i;\ i = 1, 2 \tag{13}$$

where $\mathbf{u}_i$ is the displacement of the reference point X_i. For the case of contact between the two bodies, the two points occupy the same physical space as soon as $\mathbf{x}_1 = \mathbf{x}_2$. Contact models may take into account the

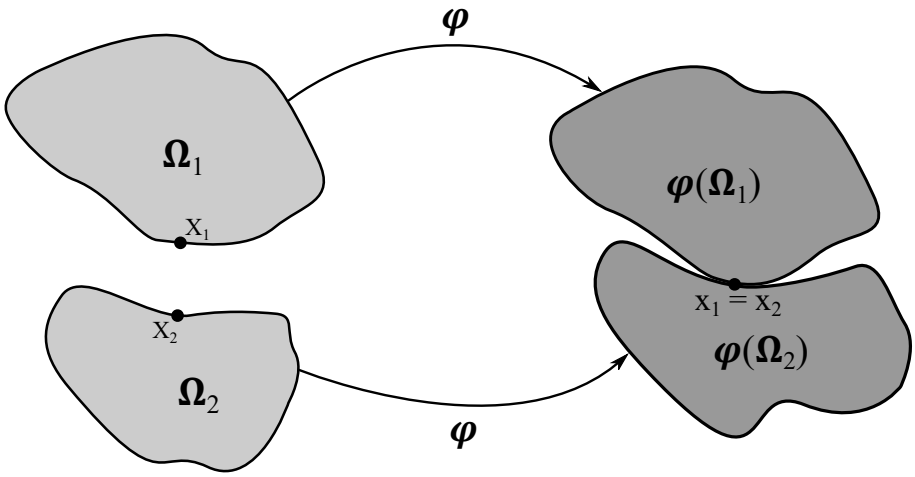

Figure 2: Reference and current configurations of two distinct bodies coming into contact

application of geometric constraints or constitutive laws at the contact interface resulting in a micromechanical approach [29]. The current study adopts geometrical constraints with a non-penetration condition. Such a condition uses a gap function g_N,

$$g_N = (\mathbf{x}_2 - \mathbf{x}_1) \cdot \mathbf{n}_1 \geq 0 \tag{14}$$

where $\mathbf{n}_1$ is the normal vector to Ω_1. For the case of geometrically linear kinematics, the gap function given in Eq. (14) becomes

$$g_N = [(\mathbf{X}_2 - \mathbf{X}_1) + (\mathbf{u}_2 - \mathbf{u}_1)] \cdot \mathbf{n}_1 \geq 0 \tag{15}$$

The above results in an alternative definition of the gap function as

$$g_N = (\mathbf{u}_2 - \mathbf{u}_1) \cdot \mathbf{n}_1 + g_{init} \geq 0 \tag{16}$$

where the initial gap between the two bodies, g_{init}, is

$$g_{init} = (\mathbf{X}_2 - \mathbf{X}_1) \cdot \mathbf{n}_1 \tag{17}$$

The system is then in a state of contact when the gap function $g_N = 0$. The normal component of the stress tensor is then the contact pressure p_N, which is equal and opposite for the two bodies at the point of contact. This leads to a set of Kuhn-Tucker type equations referred to as Hertz-Signorini-Moreau conditions [29],

$$g_N \geq 0,\ p_N \leq 0,\ g_N p_N = 0 \tag{18}$$

3.2 Weak form of contact

The resulting variational form is

$$\delta L_{int} \geq \delta L_{ext} + \delta L_c \tag{19}$$

where δL_c is the variation of the work due to contact. In the current work, the nonlinear contact problem is implicitly solved using Newton's method with the penalty approach for the treatment of the contact constraint. Thus, the work due to contact takes the form

$$L_c = \frac{1}{2} \int_{\partial\Omega_c} \epsilon_N g_N^2 dA \tag{20}$$

where $\partial\Omega_c$ is the contact surface, and ϵ_N is the penalty parameter for normal contact. The virtual variation becomes

$$\delta L_c = \int_{\partial\Omega_c} \epsilon_N g_N \delta g_N dA \tag{21}$$

3.3 Node-to-Node contact

In the node-to-node formulation, the contact constraints act at the nodal level. Based on the penalty approach, the global equilibrium equation takes the following form

$$[\mathbf{K} + \mathbf{K}^p]\mathbf{u} = \bar{\mathbf{F}} \tag{22}$$

where $\mathbf{K}^p$ is the penalty stiffness matrix. The global penalty matrix stems from the assembly of the penalty stiffness terms for a given node pair i,

$$\mathbf{k}_i^p = \epsilon_N \mathbf{n}_i^T \mathbf{n}_i \tag{23}$$

where $\mathbf{n}_i = \{n_x, n_y, n_z\}$ is the unit normal vector between the node pair i, and ϵ_N is the penalty parameter. In the current work, the penalty parameter is [30]

$$\epsilon_N \leq \frac{min(\mathbf{K} + \mathbf{K_p})}{\sqrt{N \cdot t}} \tag{24}$$

where N is the degrees of freedom of the global system, and t is the round-off error. The nodal contact force, $\mathbf{F}_i^c$, for the node pair i is

$$\mathbf{F_i^c} = \epsilon_N g_N \mathbf{n_i} \tag{25}$$

The contact force term is an addition to the external force vector, and the sum represents the right-hand side of Eq. (22), such that

$$\bar{\mathbf{F}} = \mathbf{F}^c + \mathbf{F}_{ext} \tag{26}$$

4 Numerical Examples

4.1 Preliminary assessments via Hertzian contact of two cylinders

The current example is a standard benchmark test for which an analytical solution is available and hence serves to validate the contact implementation in the CUF framework. An analytical solution exists for two parallel cylinders with a line load, which results in a state of Hertzian contact [31]. The numerical case considers two half-cylinders, as shown in Fig. 3. The mechanical characteristics are as in [10]. Both cylinders have a radius R = 8, unit thickness, Young's modulus E = 200, and Poisson's ratio ν = 0.3. The load stems from a vertical displacement, u_z = -0.01, on the upper cylinder, as shown in Fig. 3. The numerical results used two models, namely, beam theories based on CUF, and 3D FE in ABAQUS, the latter serving as a reference numerical solution. Table 1 lists the model data for the CUF and ABAQUS models.

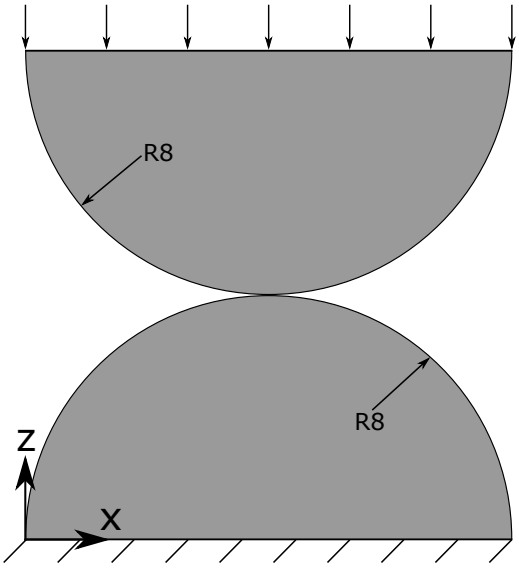

Figure 3: Half-cylinders in a state of Hertzian contact

Table 1: Modeling data for the numerical models used in the analysis of Hertzian contact

Model	Discretization of each half-cylinder	Total DOF	Time (s)
ABQ - Coarse	1,000 C3D8R	8,445	11
ABQ - Medium	6,000 C3D8R	44,583	76
ABQ - Refined	32,000 C3D8R	218,559	719
CUF - 1D	1 B4 - 128 L9	13,176	296

Figure 4 shows the displacement u_z along z at [x = 8.0, y = 0.5], while Fig. 5 shows the normal stress σ_{zz} along the same line. The 3D distribution of the vertical displacement u_z in the vicinity of the contact region is in Fig. 6. Table 2 summarizes the numerical results at the center of the contact region.

The numerical results suggest that

1. The CUF results are in good agreement with both the analytical and 3D FE solutions obtained by a

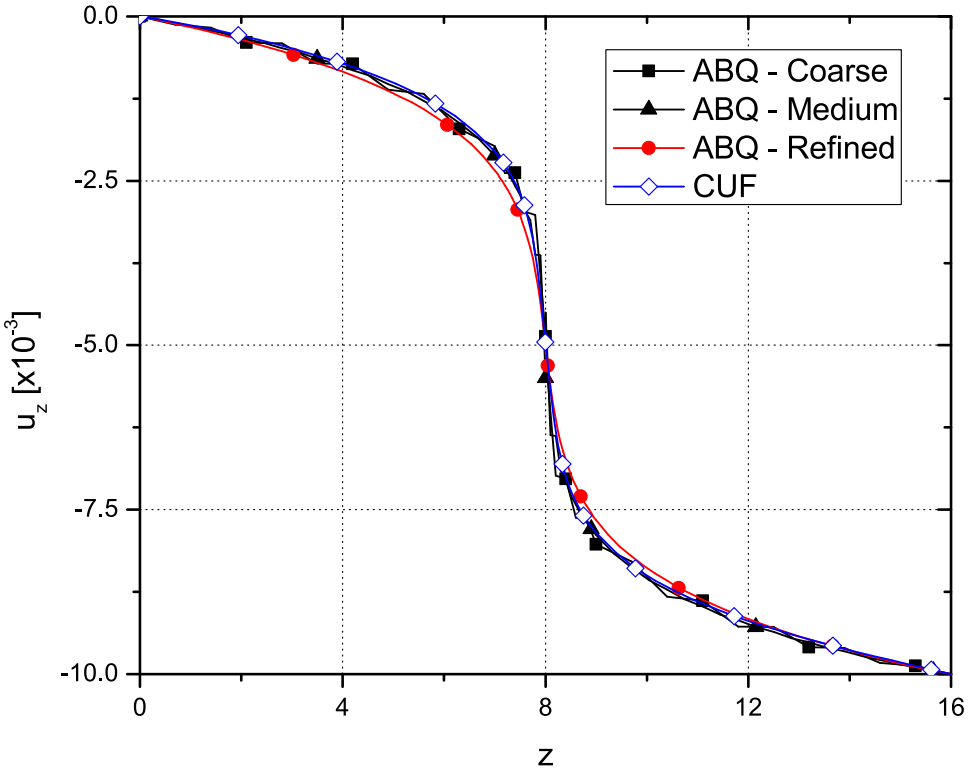

Figure 4: Vertical displacement u_z along the z-axis

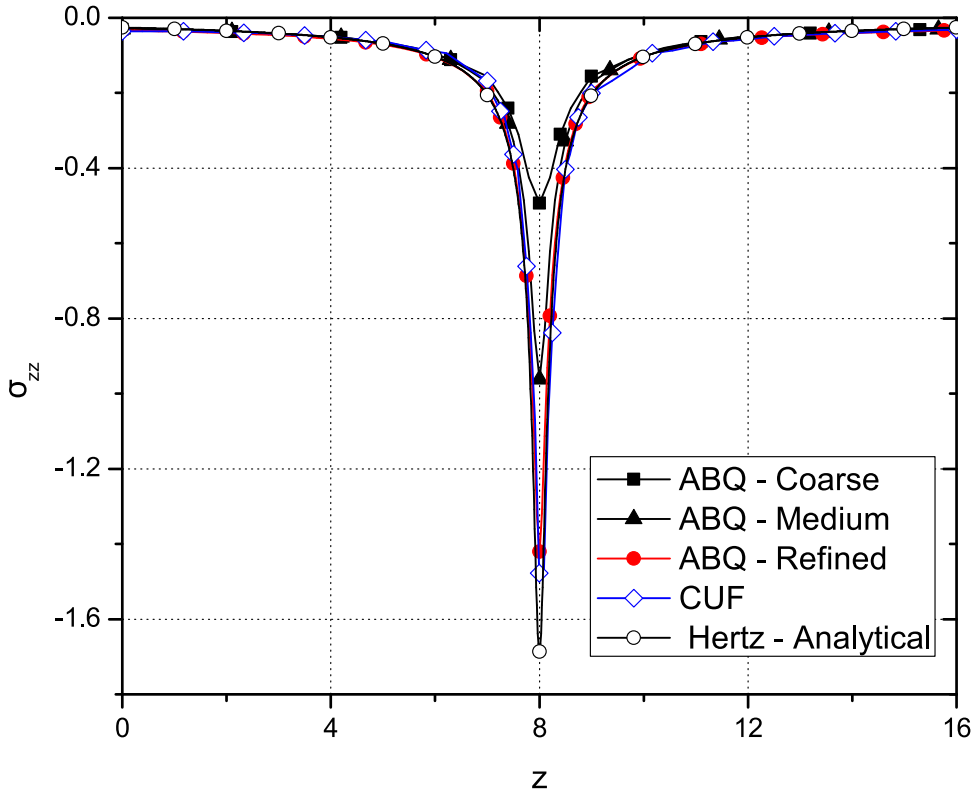

Figure 5: Normal stress σ_{zz} along the z-axis

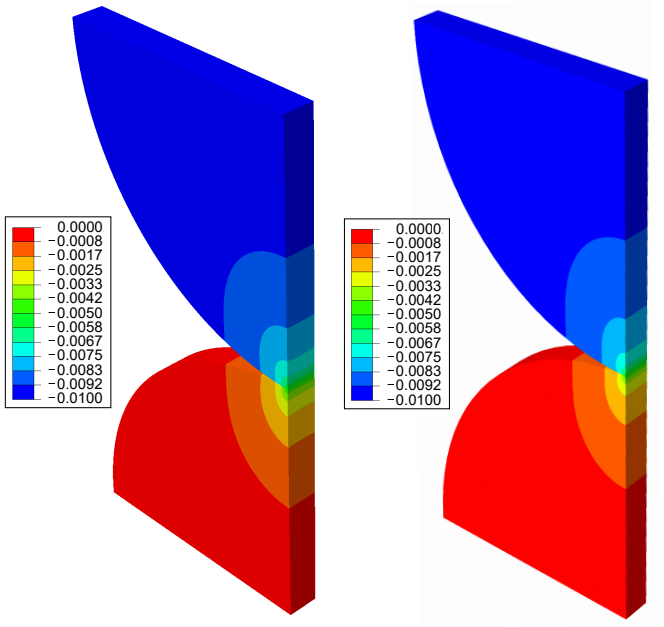

(a) CUF 1D (b) ABQ 3D

Figure 6: Distribution of the vertical displacement u_z near the contact region

Table 2: Numerical results at the center of the contact region [x = 8.0, y = 0.5, z = 8.0]

Model	σ_{zz}
ABQ - Coarse	-0.49371
ABQ - Medium	-0.96185
ABQ - Refined	-1.42374
CUF - 1D	-1.47791
Hertz - Analytical	-1.68676

3D finite element analysis. In particular, the maximum transverse axial stress is particularly demanding regarding the mesh resolution required.

2. The CUF model can capture the deformed configuration at the contact region in a computationally efficient manner, requiring about 16 times fewer DOF than a standard 3D FE. Significant advantages in the computational time are observable although, most likely, such an advantage could increase via further optimization of the CUF FE code.

3. As well known, the inclusion of the transverse stretching is decisive to detect such results.

4.2 Laminated beams in contact

The current example considers two composite laminated beams which come into contact due to an applied central deflection, as shown in Fig. 7. Each beam consists of 3 plies, [0/90/0], with each ply having a thickness of 0.001 m. The ends of both beams are clamped, and a displacement $u_z = 0.15$ m is at the mid-span of the upper beam, i.e., [x = 0.05, y = 1.0, z = 0.106]. The material system used is IM7/8552, see Table 3.

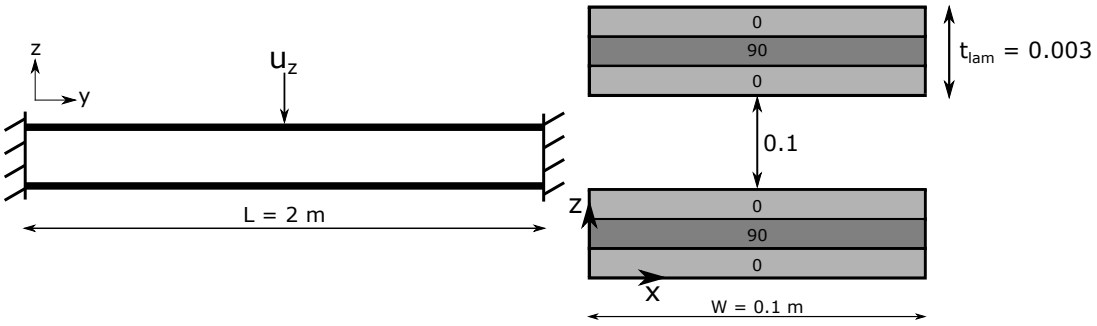

Figure 7: A schematic representation of two laminated beams coming into contact (all dimensions in m)

Table 3: Orthotropic material properties

E_1 [GPa]	E_2 [GPa]	E_3 [GPa]	G_{12} [GPa]	G_{13} [GPa]	G_{23} [GPa]	ν_{12}	ν_{13}	ν_{23}
165.0	9.0	9.0	5.6	5.6	2.8	0.34	0.34	0.5

The structural models adopted are classical beam theories - EBBT and TBT - and higher-order CUF beam models. Reference numerical solutions stemmed from 3D FE using ABAQUS. Table 4 summarizes the model data concerning the mesh and computational effort.

The results of the numerical analyses refer to the maximum applied displacement. Figure 8 shows the longitudinal displacement, u_y, and vertical deflection, u_z, along the y-axis, [x = 0.05, z = 0.003], whereas the axial stress σ_{yy} along the same line is in Fig. 9. LW indicates that the LE CUF model adopted provides a layer-wise modeling of the laminate. Figure 10 shows the u_x along the x-axis of the lower beam, [y = 1.0, z = 0.003]. The transverse shear stress, σ_{yz}, through the thickness of both beams at [x = 0.05, y = 0.8] is in Fig. 11 and its distribution through the cross-section at [y = 0.8] in Fig. 12. Tables 5 and 6 summarise the numerical results for the top and bottom beams, respectively.

Table 4: Model information for the two beams in contact

Model	Discretization of each beam	Total DOF	Time (s)
3D FE			
ABQ - Coarse	6,000 C3D8R, 1 element per ply	51,597	57
ABQ - Medium	14,400 C3D8R, 2 elements per ply	107,541	191
ABQ - Refined	43,200 C3D8R, 3 elements per ply	301,041	785
ABQ - Quadratic	6,000 C3D20R, 1 element per ply	189,945	436
1D CUF			
CUF LW	20 B4 - 12 L9	23,058	227

Table 5: Numerical results for the upper beam at the point x = 0.05, y = 0.8, z = 0.106

Model	u_y [mm]	u_z [mm]	σ_{yy} [MPa]
3D FE			
ABQ - Coarse	0.2156	-134.340	-89.1
ABQ - Medium	0.2159	-134.363	-111.7
ABQ - Refined	0.2158	-134.353	-119.1
ABQ - Quad	0.2156	-134.316	-133.7
Classical Beam Theory			
EBBT	0.2159	-134.395	-126.4
TBT	0.2159	-134.395	-126.4
CUF Layer-Wise Theory			
CUF LW	0.2157	-134.335	-126.6

Table 6: Numerical results for the lower beam at x = 0.05, y = 0.8, z = 0.003

Model	$u_y \times 10^3$ [mm]	u_z [mm]	σ_{yy} [MPa]
3D FE			
ABQ - Coarse	7.188	-44.761	-29.7
ABQ - Medium	7.193	-44.779	-37.2
ABQ - Fine	7.193	-44.776	-39.7
ABQ - Quad	7.186	-44.765	-44.5
Classical Beam Theory			
EBBT	7.198	-44.798	-42.1
TBT	7.198	-44.798	-42.1
CUF Layer-Wise Theory			
CUF LW	7.190	-44.778	-42.2

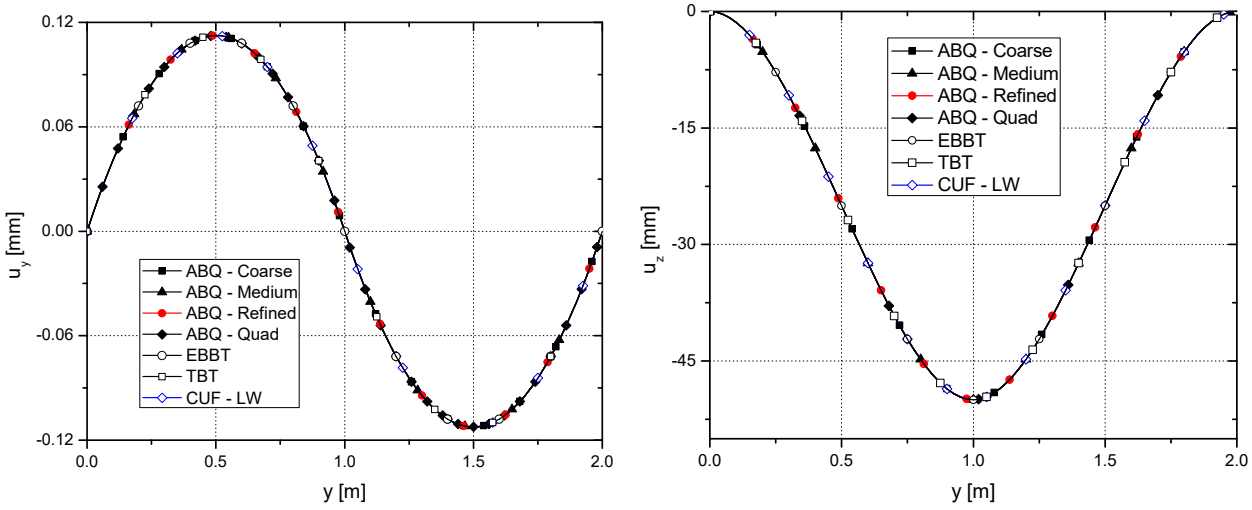

(a) u_y (b) u_z

Figure 8: Displacement components along the longitudinal axis of the lower beam

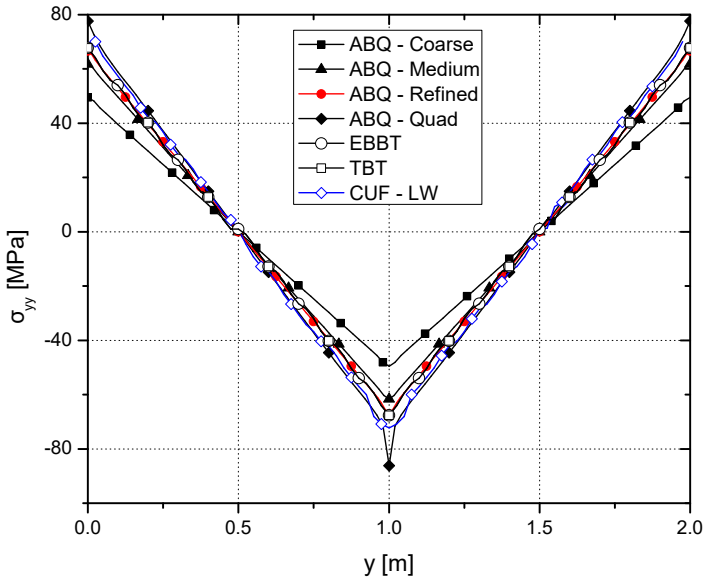

Figure 9: Axial stress σ_{yy} along the longitudinal axis of the lower beam

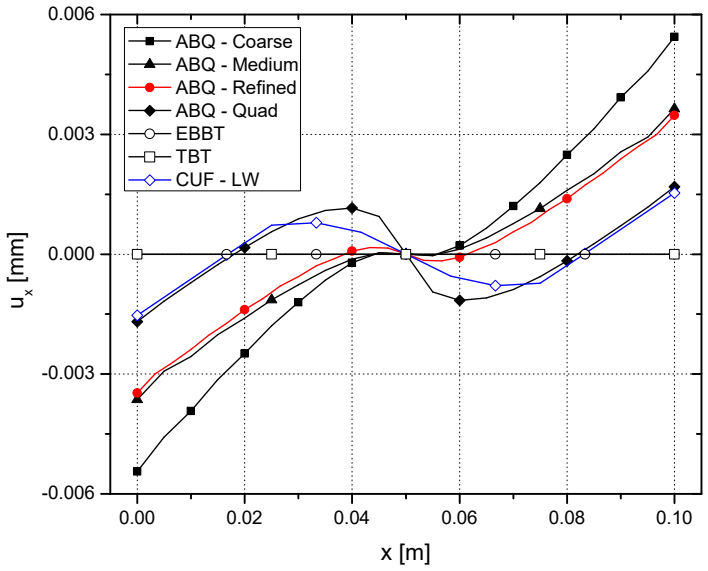

Figure 10: Transverse displacement u_x along the x-axis of the lower beam

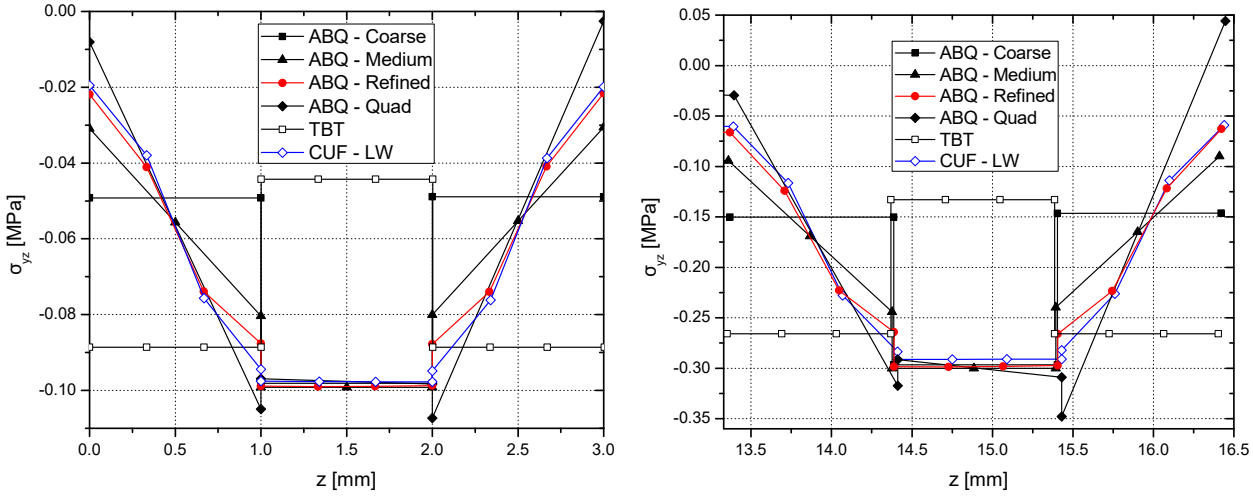

(a) σ_{yz} - lower beam (b) σ_{yz} - upper beam

Figure 11: Shear stress σ_{yz} through the thickness of the laminated beams

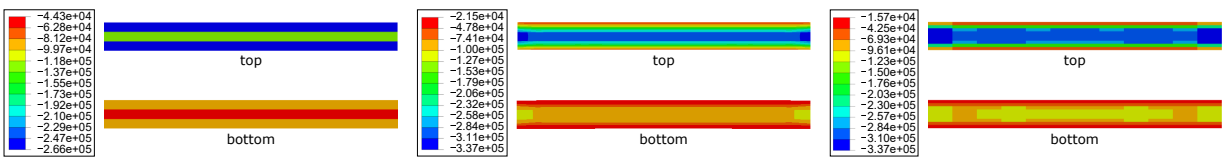

(a) TBT (b) ABQ - Refined (c) CUF - LW

Figure 12: Shear stress σ_{yz} distribution over the cross-section of the beams in contact [y = 0.8 m]

The numerical results suggest that

1. Lower-order models, i.e., EBBT and TBT, provide good accuracy concerning transverse displacement and axial stress.

2. The proper detection of transverse shear stresses requires higher-order models. Moreover, the CUF model layer-wise capabilities lead to fairly good continuity of transverse shear at the interfaces.

3. 3D FE requires multiple elements through the ply thickness to accurately capture interlaminar shear stresses leading to very high computational costs due to the aspect ratio constraints.

4. The CUF LW model requires about $21x$ fewer degrees of freedom and $6x$ less computational time, compared to a full 3D finite element analysis, for comparable quality of results.

4.3 Sandwich beam under bending

The current example considers a sandwich beam consisting of a soft foam core and composite laminated face-sheets. The beam is under a 3-point bending test with the ends clamped, and the central bending load applied via a semi-circular roller, as shown in Fig. 13. Each face-sheet is a 3-ply laminate with a [0/90/0] stacking sequence and a ply thickness of 1 mm. The composite material system is Glass-Fibre/Polyester, see Table 7. The foam core is isotropic with Young's Modulus E = 35 MPa and Poisson's ratio $\nu = 0.4$. The structural model

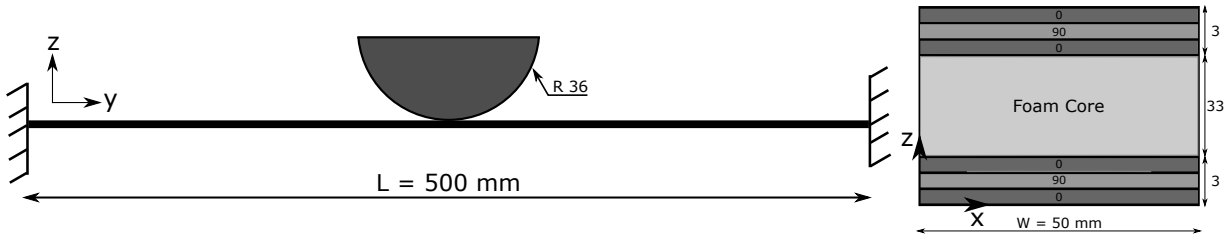

Figure 13: Doubly-clamped sandwich beam under three-point bending

Table 7: Material properties of the face-sheet used in the sandwich beam under three-point bending

Material	E_1 [GPa]	E_2 [GPa]	E_3 [GPa]	G_{12} [GPa]	G_{13} [GPa]	G_{23} [GPa]	ν_{12}	ν_{13}	ν_{23}
Glass fibre-Polyester	25.8	8.7	8.7	3.5	3.5	2.4	0.34	0.34	0.47

is 1D CUF LW, and the indenting roller is a beam with a semi-circular cross-section, oriented perpendicular to the sandwich beam. Reference numerical solutions stemmed from 3D FE analysis in ABAQUS. The modeling details for the various models are in Table 8. The results refer to the configuration in which the top surface of the beam reached u_z = -4 mm. The shear stress σ_{yz} through the thickness of the sandwich, at the point [x = 0.025, y = 0.15], is in Fig. 14. The contour plots of the transverse stretching ϵ_{zz}, axial and shear stress σ_{yy} and σ_{yz} of the cross-section at the mid-span [y = 0.25 m], are in Fig. 15, 16 and 17, respectively. The numerical results in various points of the structure are in Table 9.

The results suggest that

Table 8: Model information for the various finite element analyses of the sandwich beam under 3-point bending

Model	Sandwich beam discretisation	DOF	CPU Time (s)
3D FE			
ABQ3D - Coarse	11,200 C3D8R, 1 element per ply	45,408	40
ABQ3D - Medium	44,800 C3D8R, 2 elements per ply	153,300	320
ABQ3D - Refined	80,000 C3D8R, 4 elements per ply	261,675	832
ABQ3D - Quadratic	14,000 C3D20R, 1 element per ply	201,504	396
CUF LW			
CUF LW	10 B4 - 32 L9, 1 element per ply	14,229	279

Table 9: Numerical results at specific points of the sandwich structure as obtained by the various analyses

Model	u_y [mm] (y = 125, z = 36)	σ_{zz} [MPa]	σ_{yy} [MPa] (z = 0)
Reference 3D FE			
ABQ3D - Coarse	0.0527	-1.17	23.8
ABQ3D - Medium	0.0530	-1.28	27.1
ABQ3D - Refined	0.0531	-1.34	28.9
ABQ3D - Quad	0.0531	-1.35	30.7
CUF Layer-Wise Theory			
CUF LW	0.0553	-1.33	31.1

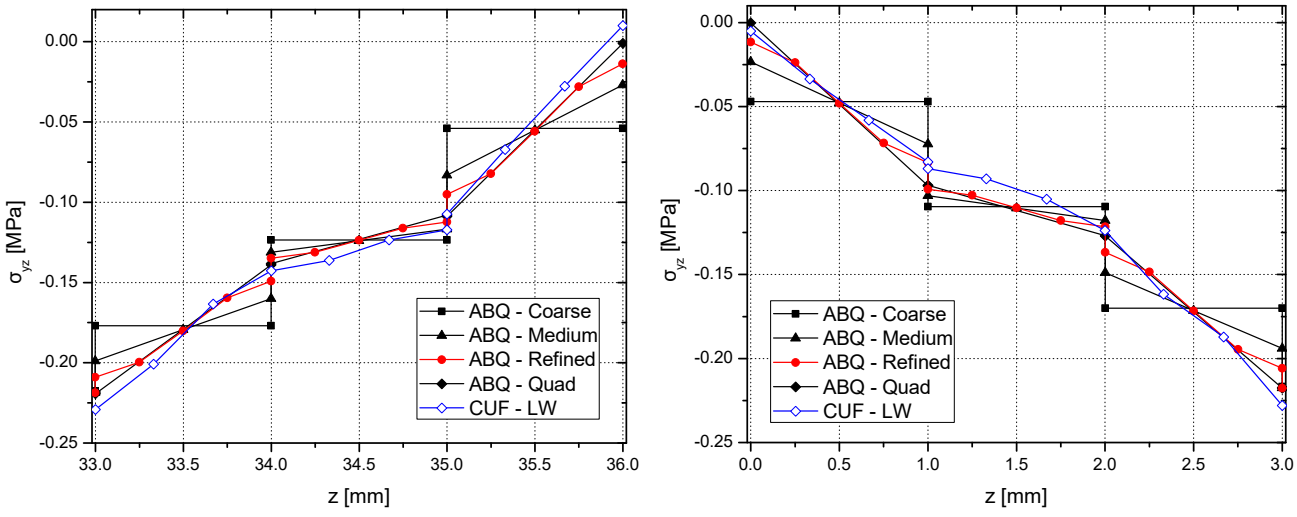

(a) top (b) bottom

Figure 14: Transverse shear stress σ_{yz} through the thickness of the sandwich outer layers

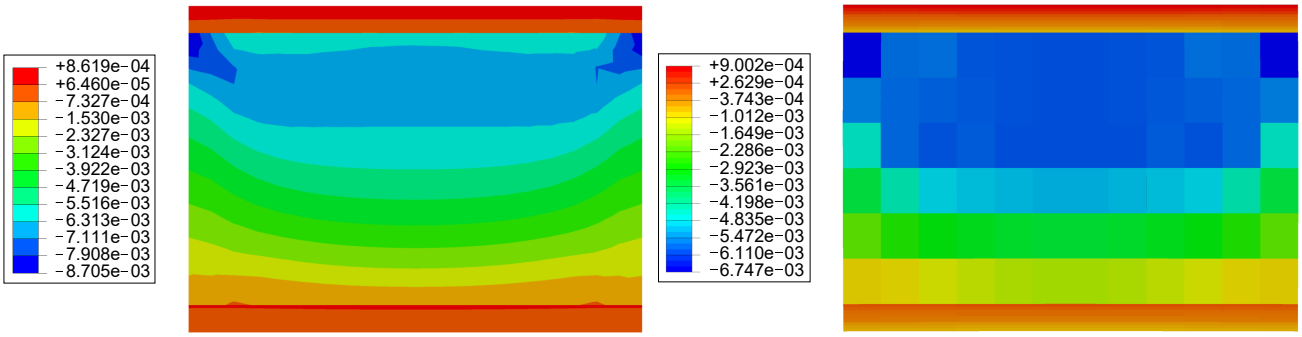

(a) ABQ - Refined (b) CUF LW

Figure 15: Transverse axial strain ϵ_{zz} distribution at the cross-section of the sandwich beam [y = 0.25 m]

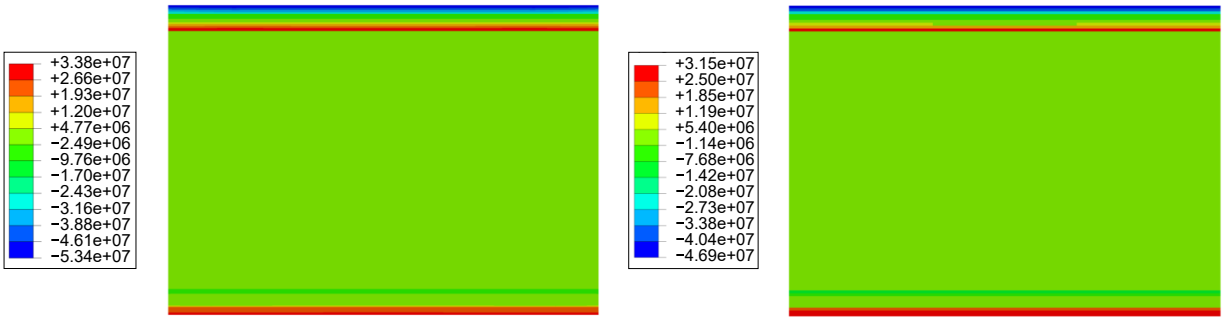

(a) ABQ - Refined (b) CUF - LW

Figure 16: Axial stress σ_{yy} distribution at the cross-section of the sandwich beam [y = 0.25 m]

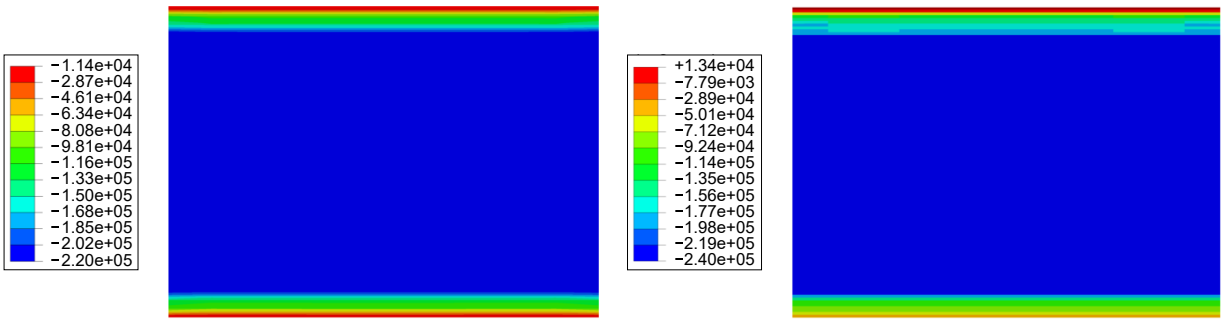

(a) ABQ - Refined (b) CUF - LW

Figure 17: Transverse shear stress σ_{yz} distribution at the cross-section of the sandwich beam [y = 0.15 m]

1. As in the previous case, the proposed formulation proved accurate in detecting strain and stress components.

2. The use of refined 1D models leads to a fairly complex cross-sectional distribution of ϵ_{zz} and as accurate as 3D FE.

3. The computational advantages of the present framework remain.

5 Conclusion

This paper has presented numerical results on contact problems of composite structures via 1D models accounting for transverse shear and stretching. Numerical assessments considered analytical solutions, classical beam theories, and 3D FE for comparison purposes. The present formulation - stemmed from the 1D CUF models - provides a layer-wise description of the multilayer structure and the full 3D strain and stress field. The numerical results suggest that

1. Classical beam theories are reliable to predict the global transverse displacement distribution but are unable to account for localized deformations that often occur in the contact region causing both local cross-sectional changes.

2. The present LW formulation provides accurate through-the-thickness strain and stress distributions with almost continuous transverse shear distributions.

3. As compared to 3D FE, 1D CUF-LW provides a two-order of magnitude reduction in the degrees of freedom and a one-order of magnitude reduction in the computational time. 3D FE requires multiple elements along the thickness to capture transverse distributions, and such a requirement combines negatively with the aspect ratio constraint.

The proper detection of the full 3D strain and stress field within the nonlinear contact framework is the first step towards the impact analysis and to detect the onset of damage and further propagations. Further works include the implementation of surface-based contact algorithms.

Acknowledgements

This research work has been carried out within the project ICONIC (Improving the Crashworthiness of Composite Transportation Structures), funded by the European Union Horizon 2020 Research and Innovation program under the Marie Skłodowska-Curie Grant agreement No. 721256, and the project FULLCOMP (Fully integrated analysis, design, manufacturing and health-monitoring of composite structures), funded by the European Union Horizon 2020 Research and Innovation program under the Marie Skłodowska-Curie Grant agreement No. 642121.

References

[1] M.A. Puso and T.A. Laursen. A mortar segment-to-segment contact method for large deformation solid mechanics. *Computer methods in applied mechanics and engineering*, 193(6-8):601–629, 2004.

[2] A. Francavilla and O.C. Zienkiewicz. A note on numerical computation of elastic contact problems. *International Journal for Numerical Methods in Engineering*, 9(4):913–924, 1975.

[3] J.T. Stadter and R.O. Weiss. Analysis of contact through finite element gaps. *Computers & Structures*, 10(6):867–873, 1979.

[4] J.O. Hallquist, G.L. Goudreau, and D.J. Benson. Sliding interfaces with contact-impact in large-scale lagrangian computations. *Computer methods in applied mechanics and engineering*, 51(1-3):107–137, 1985.

[5] P. Wriggers and J.C. Simo. A note on tangent stiffness for fully nonlinear contact problems. *Communications in Applied Numerical Methods*, 1(5):199–203, 1985.

[6] P. Papadopoulos and R.L. Taylor. A mixed formulation for the finite element solution of contact problems. *Computer Methods in Applied Mechanics and Engineering*, 94(3):373–389, 1992.

[7] J.C. Simo, P. Wriggers, and R.L. Taylor. A perturbed lagrangian formulation for the finite element solution of contact problems. *Computer methods in applied mechanics and engineering*, 50(2):163–180, 1985.

[8] G. Zavarise and P. Wriggers. A segment-to-segment contact strategy. *Mathematical and Computer Modelling*, 28(4-8):497–515, 1998.

[9] F.B. Belgacem, P. Hild, and P. Laborde. Approximation of the unilateral contact problem by the mortar finite element method. *Comptes Rendus de l'Academie des Sciences Series I Mathematics*, 324(1):123–127, 1997.

[10] T.W. McDevitt and T.A. Laursen. A mortar-finite element formulation for frictional contact problems. *International Journal for Numerical Methods in Engineering*, 48(10):1525–1547, 2000.

[11] K.A. Fischer and P. Wriggers. Frictionless 2d contact formulations for finite deformations based on the mortar method. *Computational Mechanics*, 36(3):226–244, 2005.

[12] J.H. Kim, J.H. Lim, J.H. Lee, and S. Im. A new computational approach to contact mechanics using variable-node finite elements. *International journal for numerical methods in engineering*, 73(13):1966–1988, 2008.

[13] S. Jin, D. Sohn, and S. Im. Node-to-node scheme for three-dimensional contact mechanics using polyhedral type variable-node elements. *Computer Methods in Applied Mechanics and Engineering*, 304:217–242, 2016.

[14] P. Wriggers, W.T. Rust, and B.D. Reddy. A virtual element method for contact. *Computational Mechanics*, 58(6):1039–1050, 2016.

[15] P. Wriggers and G. Zavarise. On contact between three-dimensional beams undergoing large deflections. *Communications in numerical methods in engineering*, 13(6):429–438, 1997.

[16] G. Zavarise and P. Wriggers. Contact with friction between beams in 3-d space. *International Journal for Numerical Methods in Engineering*, 49(8):977–1006, 2000.

[17] P. Litewka and P. Wriggers. Contact between 3d beams with rectangular cross-sections. *International Journal for Numerical Methods in Engineering*, 53(9):2019–2041, 2002.

[18] A.G. Neto, P.M. Pimenta, and P. Wriggers. A master-surface to master-surface formulation for beam to beam contact. part i: frictionless interaction. *Computer Methods in Applied Mechanics and Engineering*, 303:400–429, 2016.

[19] N. Silvestre and D. Camotim. First-order generalised beam theory for arbitrary orthotropic materials. *Thin-Walled Structures*, 40(9):755–789, 2002.

[20] N. Silvestre and D. Camotim. Second-order generalised beam theory for arbitrary orthotropic materials. *Thin-Walled Structures*, 40(9):791–820, 2002.

[21] W. Yu, V. V. Volovoi, D. H. Hodges, and X. Hong. Validation of the variational asymptotic beam sectional analysis. *AIAA journal*, 40(10):2105–2112, 2002.

[22] E. Carrera, M. Cinefra, M. Petrolo, and E. Zappino. *Finite element analysis of structures through unified formulation*. John Wiley & Sons, 2014.

[23] A.G. de Miguel, I. Kaleel, M. H. Nagaraj, A. Pagani, M. Petrolo, and E. Carrera. Accurate evaluation of failure indices of composite layered structures via various fe models. *Composites Science and Technology*, 167:174–189, 2018.

[24] A. Pagani and E. Carrera. Unified formulation of geometrically nonlinear refined beam theories. *Mechanics of Advanced Materials and Structures*, 25(1):15–31, 2018.

[25] M. Petrolo, M. H. Nagaraj, I. Kaleel, and E. Carrera. A global-local approach for the elastoplastic analysis of compact and thin-walled structures via refined models. *Computers & Structures*, 206:54–65, 2018.

[26] I. Kaleel, M. Petrolo, A. M. Waas, and E. Carrera. Micromechanical progressive failure analysis of fiber-reinforced composite using refined beam models. *Journal of Applied Mechanics*, 85(2):021004, 2018.

[27] E. Carrera, G. Giunta, and M. Petrolo. *Beam structures: classical and advanced theories*. John Wiley & Sons, 2011.

[28] E. Carrera and M. Petrolo. Refined beam elements with only displacement variables and plate/shell capabilities. *Meccanica*, 47(3):537–556, 2012.

[29] P. Wriggers. *Computational Contact Mechanics*. Springer-Verlag, 2006.

[30] B. Nour-Omid and P. Wriggers. A note on the optimum choice for penalty parameters. *Communications in Applied Numerical Methods*, 3(6):581–585, 1987.

[31] H. Hertz. Uber die beruhrung fester elastischer korper (on the contact of elastic solids). *J. fur die Reine Angew. Math.*, 92:156–171, 1881.